PAPER

Check for updates

Amino-functionalization enhanced CO$_2$ reduction reaction in pure water†

Junfeng Chen, Wenzhe Niu, [ID] Liangyao Xue, [ID] Kai Sun, Xiao Yang, Xinyue Zhang, Weihang Li, Shuanglong Huang, Wenjuan Shi [ID] * and Bo Zhang [ID] *

The electrochemical reduction of carbon dioxide (CO$_2$RR) to carbon monoxide represents a cost-effective pathway towards realizing carbon neutrality. To suppress the hydrogen evolution reaction (HER), the presence of alkali cations is critical, which can however lead to precipitate formation on the electrode, adversely impacting the device stability. Employing pure water as the electrolyte in zero-gap CO$_2$ electrolyzers can address this challenge, albeit at the cost of diminished catalyst performance due to the absence of alkali cations. In this study, we introduce a novel approach by implementing amino modifications on the catalyst surface to mimic the function of alkali metal cations, while simultaneously working in pure water. This modification enhances the adsorption of carbon dioxide and protons, thereby facilitating the CO$_2$RR while concurrently suppressing the HER. Utilizing this strategy in a zero-gap CO$_2$ electrolyzer with pure water as the anolyte resulted in an impressive carbon monoxide faradaic efficiency (FE$_{CO}$) of 95.5% at a current density of 250 mA cm^{-2}, while maintaining stability for over 180 hours without any maintenance.

1 Introduction

The capture, storage and utilization of carbon dioxide (CO$_2$) for the production of high-value fuels and feedstocks represents a viable strategy for mitigating carbon emissions and promoting carbon recycling.[1–5] Among the various strategies, the electrochemical reduction of CO$_2$ (CO$_2$RR) to carbon monoxide (CO) using renewable electricity stands out due to its high selectivity, relatively rapid reaction rates and low separation costs.[6–9]

A key focus in CO$_2$-to-CO conversion systems is the suppression of the hydrogen evolution reaction (HER) as a deleterious side reaction, along with overcoming the activation barrier of CO$_2$ molecules to enhance the CO selectivity under various pH conditions, including alkaline, acidic, or near-neutral environments.[10–14] These systems often depend on alkali cations (Na$^+$, K$^+$, Cs$^+$) to modify the cathode local environment, where these cations adsorb onto the Helmholtz layer, preventing proton access and thus inhibiting the HER.[15] Additionally, the hydrolysis of alkali metal cations can increase local pH levels near the cathode, thereby augmenting the CO$_2$ concentration and improving the selectivity and rate of CO

State Key Laboratory of Molecular Engineering of Polymers & Department of Macromolecular Science, Fudan University, Shanghai 200438, China
†Electronic supplementary information (ESI) available. See DOI: https://doi.org/10.1039/d4nr01416b

electrosynthesis.[16–18] However, the inevitable interaction between alkali cations and carbonate/bicarbonate ions (CO$_3^{2-}$ and HCO$_3^-$, generated from CO$_2$ and OH$^-$) leads to salt formation on the surface of the electrode. This accumulation causes blockages in the gas diffusion electrode (GDE) and cathode microchannels, culminating in premature failure of the device.[19,20] These challenges significantly hinder the industrial viability of the CO$_2$RR.

To address the problem of salt formation, recent studies have utilized pure water as the electrolyte in membrane electrode assembly (MEA) based zero-gap CO$_2$ electrolyzers.[6,21–24] These alkali cation-free systems effectively address the issue of salt deposition, demonstrating sustained stability, high carbon efficiency and reduced operational costs.[25] Yet, in such systems, the absence of alkali cations often results in the huge decrease in CO faradaic efficiency (FE$_{CO}$) due to a more favorable HER and a lower local CO$_2$ concentration.[21,22] Thus, enhancing the CO$_2$ concentration and suppressing the HER are challenging for efficient CO$_2$RR in pure water systems.

Incorporating the amino group, which functions as a Lewis base and is adept at adsorbing acidic molecules like CO$_2$, may offer a solution.[26–29] Amino-modification on mesoporous materials or metal–organic frameworks (MOFs) can enhance their ability to capture CO$_2$ and the adsorption kinetics.[30–33] This strategy is widely used in the field of CO$_2$ capture.[34] Similarly, researchers have found that modifying catalyst surfaces with amino groups can adsorb and activate CO$_2$ during
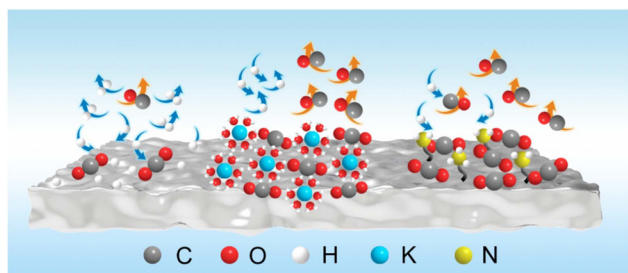
Scheme 1 Schematic of the mechanism of amino modification strategy. Similar to the effect of alkali metals, amino groups can enhance the adsorption of CO_2, and can also be protonated to adsorb protons, preventing protons from directly contacting the catalytic center.

the CO_2RR, in an alkaline electrolyte.[35–39] We therefore propose that introducing amino groups on the catalysts may enhance the CO_2RR performance in pure water.

We propose to use amino to modify catalyst surfaces, potentially to boost CO_2 adsorption on the catalysts during the electrocatalytic process. This increase in CO_2 concentration at the catalyst surface, combined with the proton-adsorbing capacity of the nitrogen atoms in amino, could effectively inhibit the HER (Scheme 1).[28,40,41] Consequently, amino modification of catalysts might serve as an innovative approach to replace the role of alkali metal cations, thereby enhancing the performance of the CO_2RR in pure water systems.

In this study, we synthesized an Ag nanocatalyst on the amino-modified carbon substrate (Ag-C-Mel). The presence of amino enhances the CO_2 adsorption capability and allows it to adsorb a certain amount of protons in pure water to suppress

the HER. *Operando* attenuated total reflection surface enhanced infrared absorption spectroscopy (ATR-SEIRAS) proved that the Ag-C-Mel exhibits stronger CO_2 adsorption and high proton adsorption capacity, ensuring its performance in the pure water system. In a zero-gap CO_2 electrolyzer, the Ag-C-Mel achieved an FE_{CO} of up to $95.5 \pm 1.0\%$ at a current density (j) of 250 mA cm^{-2}, while retaining an FE_{CO} of over 90% at 350 mA cm^{-2}. Furthermore, we sustained stable electrochemical CO synthesis for 180 hours at a current density of 250 mA cm^{-2}, operating with an FE_{CO} of over 93%.

2 Results and discussion

2.1 Synthesis and characterization of the amino-modified catalyst Ag-C-Mel

We first used melamine as the precursor to modify carbon powders (XC-72) by a one-step diazotization reaction. Subsequently, the as-prepared amino-modified carbon powders were added into a silver ammonia solution. With vigorous stirring, the silver cations (Ag$^+$) were gradually reduced, and the Ag nanoparticles were uniformly deposited onto the modified carbon supports to form the Ag-C-Mel catalyst. For comparison, the Ag-C catalyst was synthesized using the same method, using carbon powders without amino modification. X-ray powder diffraction (XRD) patterns indicated that both the Ag-C-Mel and the Ag-C catalysts possess a similar phase structure, exhibiting characteristic peaks at 38.1°, 44.3° and 64.4°, corresponding to the Ag(111), Ag(200) and Ag(220) planes (Fig. 1a), respectively. Scanning electron microscopy
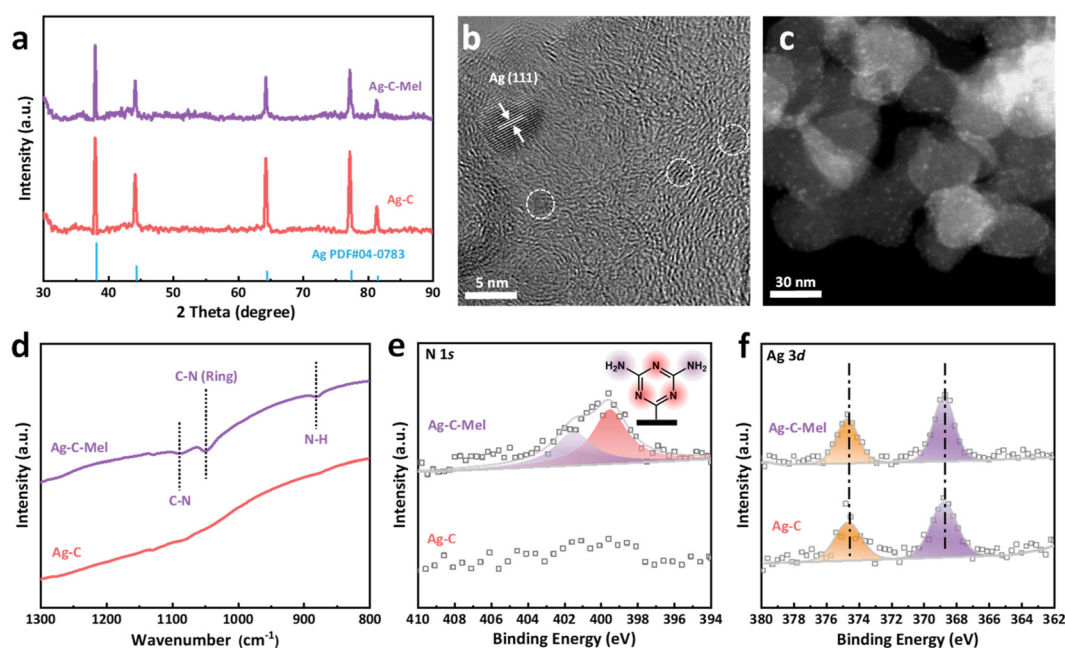

Fig. 1 Structural and compositional analysis of the Ag-C-Mel and the Ag-C catalysts. (a) XRD patterns of Ag-C-Mel and Ag-C. (b) HRTEM image of Ag-C-Mel. Scale bar, 5 nm. (c) STEM image of Ag-C-Mel. (d) Infrared spectroscopy of the Ag-C-Mel and the Ag-C samples. (e and f) High-resolution (e) N 1s spectra and (f) Ag 3d spectra of Ag-C-Mel and Ag-C.

(SEM) and transmission electron microscopy (TEM) images showed similar morphology on both samples, revealing that the amino modification did not alter the topography of the carbon powders obviously (Fig. S1, S2† and Fig. 1b, c). High-angle annular dark-field scanning TEM (HAADF-STEM) provided further insights into the microstructures of the Ag-C-Mel catalyst, where the Ag nanoparticles were distributed uniformly on the carbon supports (Fig. 1c and Fig. S2b†). High-resolution TEM (HR-TEM) images of the Ag-C-Mel revealed lattice fringe spacings of 0.237 nm, corresponding to the (111) plane of Ag, and the size of Ag nanoparticles ranged from 2 to 5 nm (Fig. 1b and Fig. S2a†). Inductively coupled plasma optical emission spectroscopy (ICP-OES) indicated a loading amount of Ag of approximately 2 wt% (Table S1†). Infrared spectroscopy (IR) revealed characteristic absorption peaks at 1086 cm^{-1}, 1048 cm^{-1} and 882 cm^{-1}, attributed to the stretching vibrations of C–N or the ring breathing vibrations of triazine (Fig. 1d).[42–46] In addition, the peak at 882 cm^{-1} could be assigned to the deformation mode of N–H.[47,48] These peaks confirm the incorporation of nitrogen-containing groups onto the Ag-C-Mel surface. We then performed X-ray photoelectron spectroscopy (XPS) to assess the electronic structure of the Ag-C-Mel sample, where two main peaks in the N 1s spectra at 399.4 eV and 401.4 eV were attributed to the sp^2 hybridized

pyridinic nitrogen (C–N=C) and amino nitrogen (Fig. 1e), respectively.[47,49,50] The peak area ratio of two N chemical environments is approximately 3 : 2. Thus, we speculate that the grafted functional groups on the modified carbon powder are 2,4-diamino-1,3,5-triazine (DT), aligning with the mechanism of *in situ* diazotization for carbon powder modification. Additionally, the Ag 3d spectra demonstrated no significant binding energy shift after the DT modification, indicating that the functional groups were primarily grafted onto the carbon powder surface without coordination with silver atoms (Fig. 1f). These characterization results confirmed that in the Ag-C-Mel catalysts, the Ag nanoparticles load uniformly on DT-group-grafted carbon supports. EDS-mapping shows that N and Ag elements were uniformly distributed on the surface of the catalyst, which proves the success of amino modification and Ag deposition (Fig. S3†).

2.2 Protonation and carbon dioxide adsorption capacity of the Ag-C-Mel catalyst

To assess the impact of DT modification on the proton adsorption capacity, we synthesized samples with different amino modification ratios by adjusting the melamine amounts (labeled as Ag-C-Mel, Ag-C-Mel$_2$ and Ag-C-Mel$_3$ with a gradient DT modification ratio). We dispersed the Ag-C, Ag-C-Mel, Ag-
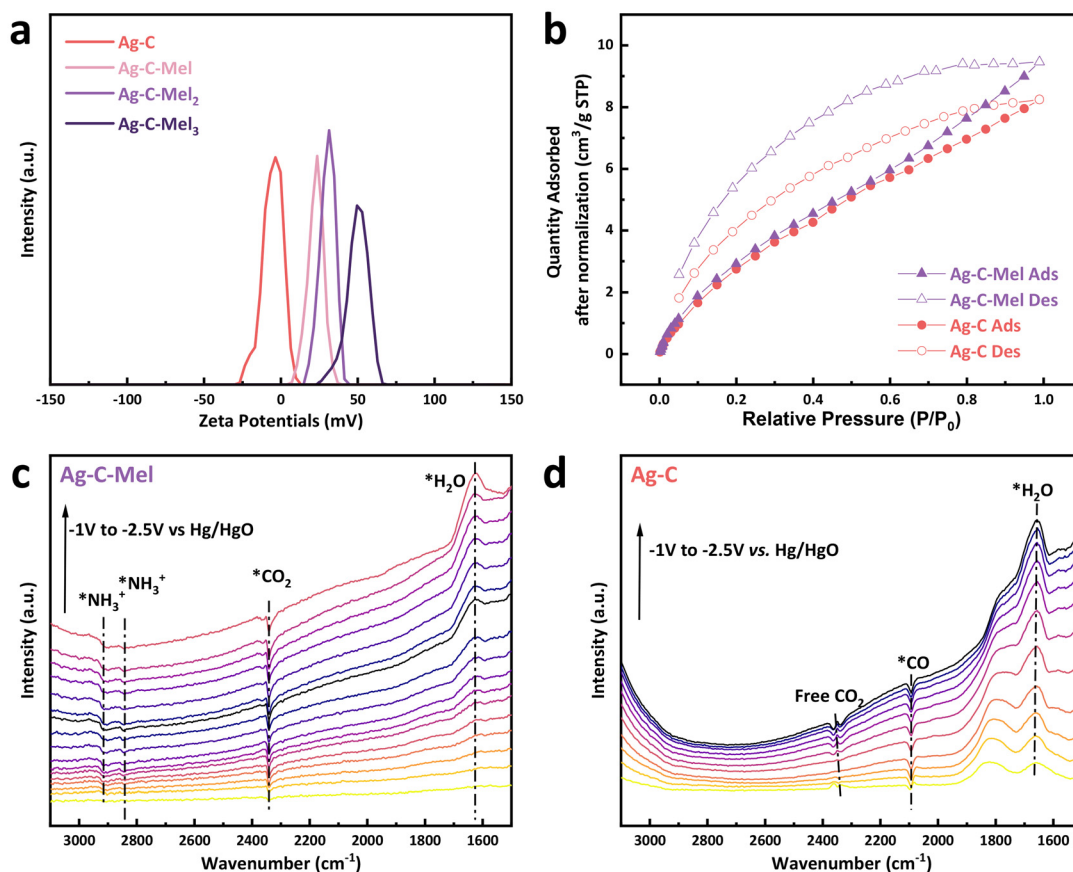
**Fig. 2** Adsorption capacity for protons and carbon dioxide of the Ag-C-Mel and the Ag-C catalysts. (a) Zeta potentiograms of catalysts with different amino modification amounts. (b) CO$_2$ adsorption and desorption isotherms of Ag-C-Mel and Ag-C at 273 K. (c and d) *Operando* ATR-SEIRAS spectra under different applied potentials using 0.5 M KHCO$_3$ electrolyte during the CO$_2$RR of (c) Ag-C-Mel and (d) Ag-C.

C-Mel$_2$ and Ag-C-Mel$_3$ samples into the ultrapure water (18.2 MΩ cm^{-1}) and measured the zeta potentials of the suspensions. In ultrapure water, there are only hydrated hydrogen ions (H$_3$O$^+$) and hydroxide ions (OH$^-$) as the ions present. The nitrogen atoms in amino groups have a pair of lone electrons capable of adsorbing protons from the solvent, leading to protonation and consequently a relatively positive surface charge on the catalyst.[51–54] As the DT modification degree increases, the zeta potential of the catalyst powder gradually increased, indicating an enhanced ability to adsorb protons, confirming the effectiveness of melamine modification in attracting protons (Fig. 2a). In contrast, unmodified carbon powder typically carries a slight negative charge due to the presence of small amounts of hydroxyl and carboxyl groups on its surface.[55,56]

To investigate the impact of amino modification on the CO$_2$ adsorption capacity of catalysts, we analyzed the CO$_2$ adsorption–desorption isotherms of the catalysts at 273 °C (Fig. 2b). We discovered that the Ag-C-Mel exhibited a stronger CO$_2$ adsorption capability, with a maximum adsorption value of 9.46 cm^3 g^{-1}, approximately 15% higher than that of Ag-C (8.25 cm^3 g^{-1}). Notably, during the desorption process, as the CO$_2$ partial pressure gradually decreased, Ag-C-Mel maintained a stronger CO$_2$ retention ability, retaining over 99% of its maximum adsorption capacity even when the relative partial pressure dropped to 0.78, revealing an enhanced CO$_2$ adsorption effect of the amino modification (Fig. S4†). This is also consistent with the CO$_2$ temperature programmed desorption (CO$_2$-TPD) results, where the main peak was higher with the amino modification, indicating a greater adsorption quantity on the Ag-C-Mel sample (Fig. S5†). Additionally, electrochemical impedance spectroscopy (EIS) shows that R_{ct} values of the Ag-C-Mel (203 Ω) sample were lower than that of Ag-C (296 Ω), demonstrating faster charge transfer on the catalyst surface of Ag-C-Mel compared to Ag-C (Fig. S6†).

Furthermore, we employed *operando* ATR-SEIRAS to monitor changes in the adsorbed species and intermediates during the CO$_2$RR conditions (Fig. 2c and d). We observed that the peaks at ∼2915 cm^{-1} and ∼2843 cm^{-1} (which are attributed to N–H stretching vibrations of –NH$_3^+$) progressively strengthen as the potential shifts negatively, suggesting that the protonation degree of amino groups increases as the scanning biases become larger.[57–60] In contrast, the –NH$_3^+$ peaks are absent in the Ag-C sample. Additionally, the peak located at ∼2343 cm^{-1} is attributed to the adsorbed CO$_2$.[61] The Ag-C-Mel sample showed a significant CO$_2$ adsorption capacity that increased with negatively shifted potential, demonstrating the enhanced CO$_2$ adsorption ability with DT modification. In contrast, there was only a double peak on the Ag-C catalyst at even higher potentials, attributed to the presence of free CO$_2$ in the system. Instead, Ag-C exhibited a strong absorption peak at around 2093 cm^{-1}, due to the stretching vibration of C–O in the adsorbed *CO.[61,62] This indicates a strong adsorption effect of the Ag-C sample with the product CO, which hinders CO release and suppresses CO$_2$RR kinetics.
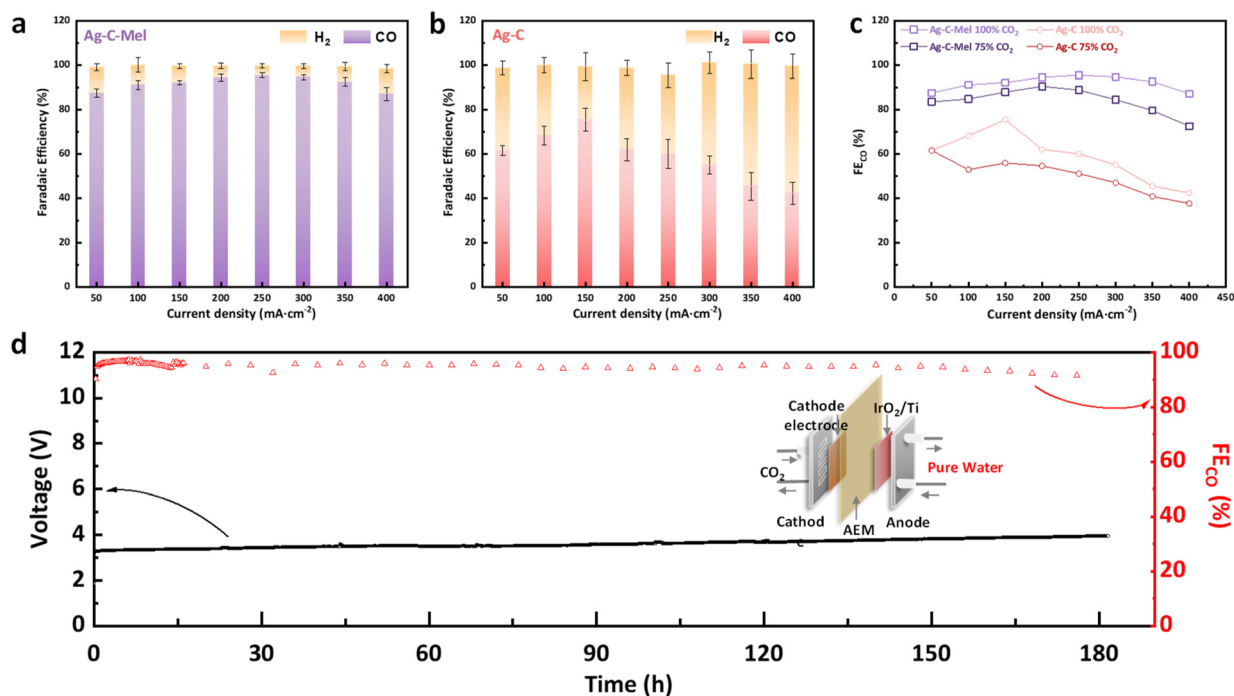
Fig. 3 The CO$_2$RR performance of Ag-C-Mel and Ag-C in a zero-gap CO$_2$ electrolyzer utilizing pure water. (a and b) CO$_2$RR product distribution under different current densities for (a) Ag-C-Mel and (b) Ag-C. (c) FE$_{CO}$ of Ag-C-Mel and Ag-C at different CO$_2$ partial pressures. (d) Continuous 180 h measurement of Ag-C-Mel at a current density of 250 mA cm^{-2}. Error bars in (a and b) correspond to the standard deviation of at least three independent measurements.

2.3 Performance of CO_2 to CO electroreduction

We utilized a zero-gap electrolyzer with ultrapure water as the anolyte to assess the CO_2-to-CO electrosynthesis performance on the Ag-C-Mel and the Ag-C catalysts (Fig. 3a and b). The FE for the products at various current densities shows that for both Ag-C-Mel and Ag-C, the CO_2RR products consist solely of H_2 and CO. The FE_{CO} from both catalysts initially increased with the rise of applied current density within the zero-gap electrolyzer, followed by a decrease. Notably, the Ag-C-Mel achieved its highest FE_{CO} of 95.5 ± 1.0% at a current density of 250 mA cm^{-2}, and at a current density of 350 mA cm^{-2}, 92.6 ± 1.9% FE_{CO} remained still. In contrast, the Ag-C catalyst exhibited the highest FE_{CO} of 75.5 ± 5.2% at 150 mA cm^{-2}, and the FE_{CO} dropped quickly below 50% at higher current densities (>350 mA cm^{-2}). Besides, we conducted CO_2RR measurement on the C-Mel without Ag nanoparticles deposited, and no carbon-based products were detected (Fig. S7a†). This further indicates that the amino-modification only changes the reaction environment around active Ag sites during the CO_2RR.

Furthermore, we assessed the CO_2RR performance of the two samples under varying CO_2 partial pressures (Fig. S8† and Fig. 3c). We altered the CO_2 partial pressures by adjusting the proportion of CO_2 in the mixture with argon gas (100%, 75%, 50%). Across all tested current densities and partial pressures, the FE_{CO} value of Ag-C-Mel was consistently higher than that of Ag-C. Reducing the CO_2 partial pressure decreased the FE_{CO} value, but for Ag-C-Mel, the decrease was under 15% at 75% CO_2 pressure. Notably, at current densities below 250 mA cm^{-2}, this decrease ranged only between 4% and 7% (Fig. S9†). We attribute this enhanced performance to the improved CO_2 adsorption due to the amino modification.

Finally, we evaluated the long-period stability of the Ag-C-Mel catalyst (Fig. 3d). The Ag-C-Mel catalyst was able to operate continuously for over 180 hours at a current density of 250 mA cm^{-2} with an average FE_{CO} of 95%. In contrast, the performance of the Ag-C catalyst severely deteriorated within two hours, with its FE_{CO} rapidly falling from 57% to 38% (Fig. S10†). These results indicated that amino modification on the catalyst surface could enable stable adsorption of protons and favor the CO_2RR with high FE_{CO}. Meanwhile, Ag-C-Mel can maintain its structure, morphology, and valence states after a long-term stability test (Fig. S11–S13†).

3 Conclusion

In this work, we proposed a strategy of introducing amino modification on the catalyst surface instead of alkali metal cations to avoid salt precipitation. In light of this, we synthesized an amino-modified silver-based catalyst (Ag-C-Mel) and utilized it in a zero-gap electrolyzer for CO_2-to-CO electrosynthesis with pure water as the electrolyte. Structural characterization revealed that the amino groups were grafted onto the carbon substrate in the form of the 2,4-diamino-1,3,5-triazine species without adversely affecting the Ag nanoparticles. The *operando* spectroscopy results indicated that the amino

modification enhanced the CO_2 adsorption capacity and imparted the ability to adsorb protons, thus inhibiting the HER. The Ag-C-Mel catalyst achieved a maximum FE_{CO} of 95.5 ± 1.0% at 250 mA cm^{-2} and maintained over 93% FE_{CO} stability for 180 hours without any maintenance. This achievement offers insights into the preparation of catalysts for zero-gap CO_2 electrolyzers in pure water systems.

Author contributions

B.Z. and W.S. supervised the project. J.C. conceived the idea and carried out most of the experiments. J.C. and W.N. performed ATR-SEIRAS measurement. L.X. provided suggestions on the experimental operations. K.S. and X.Y. performed XRD measurement. J.C. and X.Z. performed zeta-nano potential measurement. W.L., S.H. and W.S. assisted with the data analyses and discussions. J.C., W.N. W.S. and B.Z. co-wrote the manuscript. All authors discussed the results and assisted during manuscript preparation.

Data availability

The data that support the findings of this study are available in the ESI† of this article or from the corresponding author upon request.

Conflicts of interest

The authors declare no conflict of interest.

Acknowledgements

References

1 Z. W. Seh, J. Kibsgaard, C. F. Dickens, I. Chorkendorff, J. K. Nørskov and T. F. Jaramillo, *Science*, 2017, **355**, eaad4998.
2 A. R. Nihmiya, R. M. H. H. Jayarathne and A. H. L. R. Nilmini, *Asian J. Chem.*, 2023, **35**, 2031–2047.
3 J.-L. Kang, D. S.-H. Wong, S.-S. Jang and C.-S. Tan, *Int. J. Greenhouse Gas Control*, 2016, **46**, 228–239.
4 C. Hyeonuk, L. Dong-Kyu, H. Mi-Kyung, J. Gnanaprakasam, S. Subramani, K. Jin Hyeok, K. Jung Kyu, C. Hoonsung and S. Uk, *J. Electrochem. Soc.*, 2020, **167**, 164503.
5 S. C. Jesudass, S. Surendran, G. Janani, T. H. Kim and U. Sim, *Adv. Energy Mater.*, 2023, **13**, 2301918.

6   Y. Li, H. Wang, X. Yang, T. O'Carroll and G. Wu, *Angew. Chem., Int. Ed.*, 2024, **63**, e202317884.

7   Y. Y. Birdja, E. Pérez-Gallent, M. C. Figueiredo, A. J. Göttle, F. Calle-Vallejo and M. T. M. Koper, *Nat. Energy*, 2019, **4**, 732–745.

8   M. Jouny, W. Luc and F. Jiao, *Ind. Eng. Chem. Res.*, 2018, **57**, 2165–2177.

9   S. Jin, Z. Hao, K. Zhang, Z. Yan and J. Chen, *Angew. Chem., Int. Ed.*, 2021, **60**, 20627–20648.

10 L. Zhang, J. Feng, S. Liu, X. Tan, L. Wu, S. Jia, L. Xu, X. Ma, X. Song, J. Ma, X. Sun and B. Han, *Adv. Mater.*, 2023, **35**, 2209590.

11 J. Chen, X. Wei, R. Cai, J. Ren, M. Ju, X. Lu, X. Long and S. Yang, *ACS Mater. Lett.*, 2022, **4**, 497–504.

12 B. Zhang, J. Zou, Z. Chen, W. Yan, W. Liu, C. Dong, D. Cai, Q. Zhang, Y. Wang and S. Xie, *Next Nanotechnol.*, 2023, **2**, 100014.

13 Y. Ma, W. Niu, W. Shi, X. Huang, Y. Liu, J. Chen, L. Xue and B. Zhang, *J. Mater. Chem. A*, 2023, **11**, 12114–12120.

14 X. Huang, Y. Jia, S. Lee, Z. Chen and J. Xu, *Chem. Eng. J.*, 2024, **489**, 151411.

15 J. Gu, S. Liu, W. Ni, W. Ren, S. Haussener and X. Hu, *Nat. Catal.*, 2022, **5**, 268–276.

16 M. R. Singh, Y. Kwon, Y. Lum, J. W. Ager III and A. T. Bell, *J. Am. Chem. Soc.*, 2016, **138**, 13006–13012.

17 F. Zhang and A. C. Co, *Angew. Chem., Int. Ed.*, 2020, **59**, 1674–1681.

18 J. E. Huang, F. Li, A. Ozden, A. Sedighian Rasouli, F. P. García de Arquer, S. Liu, S. Zhang, M. Luo, X. Wang, Y. Lum, Y. Xu, K. Bertens, R. K. Miao, C.-T. Dinh, D. Sinton and E. H. Sargent, *Science*, 2021, **372**, 1074–1078.

19 Y. Xu, J. P. Edwards, S. Liu, R. K. Miao, J. E. Huang, C. M. Gabardo, C. P. O'Brien, J. Li, E. H. Sargent and D. Sinton, *ACS Energy Lett.*, 2021, **6**, 809–815.

20 H.-G. Qin, F.-Z. Li, Y.-F. Du, L.-F. Yang, H. Wang, Y.-Y. Bai, M. Lin and J. Gu, *ACS Catal.*, 2023, **13**, 916–926.

21 B. Endrődi, A. Samu, E. Kecsenovity, T. Halmágyi, D. Sebők and C. Janáky, *Nat. Energy*, 2021, **6**, 439–448.

22 Z. Yin, H. Peng, X. Wei, H. Zhou, J. Gong, M. Huai, L. Xiao, G. Wang, J. Lu and L. Zhuang, *Energy Environ. Sci.*, 2019, **12**, 2455–2462.

23 C. P. O'Brien, R. K. Miao, S. Liu, Y. Xu, G. Lee, A. Robb, J. E. Huang, K. Xie, K. Bertens, C. M. Gabardo, J. P. Edwards, C.-T. Dinh, E. H. Sargent and D. Sinton, *ACS Energy Lett.*, 2021, **6**, 2952–2959.

24 W. Li, Z. Yin, Z. Gao, G. Wang, Z. Li, F. Wei, X. Wei, H. Peng, X. Hu, L. Xiao, J. Lu and L. Zhuang, *Nat. Energy*, 2022, **7**, 835–843.

25 J. Y. Zhao, Y. Liu, W. Li, C. F. Wen, H. Q. Fu, H. Y. Yuan, P. F. Liu and H. G. Yang, *Chem. Catal.*, 2023, **3**, 100471.

26 A. Rehman, S. Farrukh, A. Hussain, X. Fan and E. Pervaiz, *Environ. Sci. Pollut. Res.*, 2019, **26**, 36214–36225.

27 I. Taniguchi, K. Kinugasa, M. Toyoda and K. Minezaki, *Sci. Technol. Adv. Mater.*, 2017, **18**, 950–958.

28 A. E. K. Sundén, K. Støchkel, P. Hvelplund, S. Brøndsted Nielsen, B. Dynefors and K. Hansen, *J. Chem. Phys.*, 2018, **148**, 184306.

29 S. Khaheshi, S. Riahi, M. Mohammadi-Khanaposhtani and H. Shokrollahzadeh, *Ind. Eng. Chem. Res.*, 2019, **58**, 8763–8771.

30 S. Y. W. Chai, L. H. Ngu and B. S. How, *Greenhouse Gases: Sci. Technol.*, 2022, **12**, 394–427.

31 J. Senith Ravishan Fernando, S. S. Asaithambi and S. Maruti Chavan, *ChemPlusChem*, 2024, e202400107.

32 V. Neubertová, V. Švorčík and Z. Kolská, *Microporous Mesoporous Mater.*, 2024, **366**, 112956.

33 Z. Tan, J. Zhang, Y. Yang, J. Zhong, Y. Zhao, J. Hu, B. Han and Z. Chen, *J. Am. Chem. Soc.*, 2023, **145**, 21983–21990.

34 A. A. Azmi and M. A. A. Aziz, *J. Environ. Chem. Eng.*, 2019, **7**, 103022.

35 A. Bohan, X. Jin, M. Wang, X. Ma, Y. Wang and L. Zhang, *J. Colloid Interface Sci.*, 2024, **654**, 830–839.

36 Y. Zhou, H. Qi, J. Wu, H. Huang, Y. Liu and Z. Kang, *Adv. Funct. Mater.*, 2022, **32**, 2113335.

37 Y.-Y. Liu, J.-R. Huang, H.-L. Zhu, P.-Q. Liao and X.-M. Chen, *Angew. Chem., Int. Ed.*, 2023, **62**, e202311265.

38 Y. Wang, J. Zhao, C. Cao, J. Ding, R. Wang, J. Zeng, J. Bao and B. Liu, *ACS Catal.*, 2023, **13**, 3532–3540.

39 Z. Liu, X. Han, J. Liu, S. Chen, S. Deng and J. Wang, *ACS Appl. Mater. Interfaces*, 2024, **16**, 28655–28663.

40 C.-K. Lin, R. Shishido, Q.-R. Huang, A. Fujii and J.-L. Kuo, *Phys. Chem. Chem. Phys.*, 2020, **22**, 22035–22046.

41 A. M. Navarro-Suárez, J. Carretero-González, T. Rojo and M. Armand, *J. Mater. Chem. A*, 2017, **5**, 23292–23298.

42 M. K. Marchewka, *Mater. Sci. Eng., B*, 2002, **95**, 214–221.

43 D. Thastum Bach, F. Hegelund, J. A. Beukes, F. M. Nicolaisen and M. H. Palmer, *J. Mol. Spectrosc.*, 1999, **198**, 77–93.

44 D. Zeroka, J. O. Jensen and A. C. Samuels, *J. Mol. Struct.: THEOCHEM*, 1999, **465**, 119–139.

45 L. Costa and G. Camino, *J. Therm. Anal.*, 1988, **34**, 423–429.

46 L. Segal and F. V. Eggerton, *Appl. Spectrosc.*, 1961, **15**, 116–117.

47 J. Zhang and F. Huang, *Appl. Surf. Sci.*, 2015, **358**, 287–295.

48 B. Zhu, P. Xia, W. Ho and J. Yu, *Appl. Surf. Sci.*, 2015, **344**, 188–195.

49 H. Che, G. Che, P. Zhou, C. Liu, H. Dong, C. Li, N. Song and C. Li, *Chem. Eng. J.*, 2020, **382**, 122870.

50 X. Chen, Y. Jin, P. Huang, Z. Zheng, L.-P. Li, C.-Y. Lin, X. Chen, R. Ding, J. Liu and R. Chen, *Appl. Catal., B*, 2023, **340**, 123235.

51 Z. Li, D. Nanxi, W. Zhi and Z. Song, *J. Membr. Sci.*, 2023, **688**, 122129.

52 Z. Zhao, N. Di, Z. Zha, J. Wang, Z. Wang and S. Zhao, *ACS Appl. Mater. Interfaces*, 2023, **14**, 48695–48704.

53 M. Li, Z. Lv, J. Zheng, J. Hu, C. Jiang, M. Ueda, X. Zhang and L. Wang, *ACS Sustainable Chem. Eng.*, 2016, **5**, 784–792.

54 C. Huang, X. Zhao, Y. Hao, Y. Yang, Y. Qian, G. Chang, Y. Zhang, Q. Tang, A. Hu, Z. Liu and X. Chen, *J. Mater. Chem. A*, 2022, **10**, 6636–6640.

55 C. Lafforgue, F. Maillard, V. Martin, L. Dubau and M. Chatenet, *ACS Catal.*, 2019, **9**, 5613–5622.

56 F. Maillard, W. O. Silva, L. Castanheira, L. Dubau and F. H. B. Lima, *ChemPhysChem*, 2019, **20**, 3106–3111.

57 C. Brissette and C. Sandorfy, *Can. J. Chem.*, 1960, **38**, 34–44.

58 L. Pallavi, J. Tonannavar and J. Tonannavar, *J. Mol. Struct.*, 2020, **1211**, 128085.

59 M. D. Prabhu, J. Tonannavar Yenagi, V. Kamat and J. Tonannavar, *J. Mol. Struct.*, 2020, **1218**, 128495.

60 Z. Yermiyahu, I. Lapides and S. Yariv, *Colloid Polym. Sci.*, 2008, **286**, 1233–1242.

61 S. Zhu, B. Jiang, W.-B. Cai and M. Shao, *J. Am. Chem. Soc.*, 2017, **139**, 15664–15667.

62 E. P. Delmo, Y. Wang, Y. Song, S. Zhu, H. Zhang, H. Xu, T. Li, J. Jang, Y. Kwon, Y. Wang and M. Shao, *J. Am. Chem. Soc.*, 2024, **146**, 1935–1945.